Chemical Papers (2022) 76:4795–4805
https://doi.org/10.1007/s11696-022-02204-1

ORIGINAL PAPER

Magnetite nanoparticles-incorporated composite thin-film nanofiltration membranes based on cellulose nitrate substrate

Majed M. Alghamdi[1] · Adel A. El-Zahhar[1] · Norah M. Alshahrani[2]

Received: 30 January 2022 / Accepted: 29 March 2022 / Published online: 19 April 2022

Abstract

Thin-film composite nanofiltration membranes were prepared through interfacial polymerization of trimesoyl chloride (TMC), polyvinylpyrrolidone (PVP), and magnetite nanoparticles (MNPs) on the upper surface of porous cellulose nitrate (CN) membranes. Structural and morphological properties of the prepared membranes (CN-TMC/PVP–MNP) were analyzed using FTIR, SEM, membrane contrast and AFM. The effects of reaction time, PVP concentration, and MNPs content on membrane performance were studied. Surface hydrophilicity and membrane performance were analyzed by measuring pure water contact angle, zeta potential, pure water permeation flux (PWP), and solute rejections. The CN-TMC/PVP–MNPs membranes exhibited a smooth surface and diverse surface functionalities following interfacial polymerization. The membrane surface charge was strongly affected by the presence of MNPs. Although PWP decreased with increasing MNPs content up to 0.10 wt%, Na_2SO_4 and NaCl rejections increased with increasing MNPs content, reaching, respectively, 96.8% and 76.6% at 0.1 wt% MNPs content. Moreover, the increases in steady-state flux and FRRs with increasing MNPs content, reflecting the improvement of antifouling behavior, stability, and durability, indicating their possible application for water desalination and treatment.

Keywords Thin-film composite · Nanofiltration membrane · Cellulose nitrate · Magnetite

Introduction

As a result of population growth and rapid development, freshwater scarcity has become a major current challenge. To overcome this, seawater desalination is essential in some countries as an alternative to generate freshwater (Geoffrey et al. 2010; Chung et al. 2012), and membrane filtration is an important technique to realize this. In particular, nanofiltration (NF) has found wide applications in seawater desalination and water decontamination, in addition to its industrial, pharmaceutical, and biological uses (Bai et al. 2019; Ma et al. 2019; Kim et al. 2018; Xu et al. 2017; Ye et al. 2017; Rathore and Shirke 2011; Zhao et al. 2018). However, for their desalination application, NF membranes must possess certain properties such as high rejection, permeability, operational stability, and mechanical strength. Accordingly, the use of active separation surface thin-film nanocomposite for NF has been explored (Lau et al. 2012).

Thin-film composite (TFC) membranes with desired structural properties of the surface thin-film can be fabricated using different processes, such as interfacial polymerization, dip coating, and layer-by-layer (LbL) assembly (Wei et al. 2013; Han et al. 2014; Joseph et al. 2015). In addition, the incorporation of nanomaterials can effectively improve material properties. Therefore, TFC membranes containing different materials have been investigated. For instance, TFC membranes containing graphene oxide showed better membrane performance and higher filtration efficiency (Cheng et al. 2021; Kumar et al. 2019). Moreover, TFC membranes fabricated from polysulfone embedded with zeolite nanoparticles through interfacial polymerization of the polyamide layer showed increased surface roughness, water permeability, and membrane performance (Dong

✉ Adel A. El-Zahhar
elzahhar@kku.edu.sa

Majed M. Alghamdi
mmalghamdi@kku.edu.sa

Norah M. Alshahrani
noo0oorah2011@hotmail.com

[1] Department of Chemistry, Faculty of Science, King Khalid University, P.O. Box 9004, Abha 61413, Saudi Arabia

[2] Department of Chemistry, College of Science, Bisha University, P.O. Box 551, Bisha 61922, Saudi Arabia

et al. 2016). Likewise, NF membranes fabricated through interfacial polymerization of trimesoyl chloride (TMC) and disodium-3-3′-disulfone-4-4′-dichlorodiphenylsulfone (S-DADPS)/piperazine (PIP) on porous polysulfone showed increased flux, dye rejection, and pH and temperature resistance (Ormanci et al. 2020). Furthermore, variation of the S-DADPS/PIP ratio strongly affected membrane performance; as such, membranes with the S-DADPS/PIP ratio of 80/20 showed markedly improved water flux, although their salt or dye rejection remained unaffected. In another study, TFC membranes were fabricated via LbL interfacial polymerization of polyethyleneimine (PEI) onto the polyamide surface, followed by *N*-methylation and quaternization using 3-bromopropionic acid (Deng et al. 2021); water permeation ability of the produced membrane was improved by 11.6%, and these surface-modified membranes showed improved ion selectivity and rejection for divalent ions. TFC membranes prepared via interfacial polymerization of sericin polymer and TMC onto a commercial porous polysulfone support exhibited a smooth surface, with an isoelectric point of pH 4.1 and salt rejection of, respectively, 22.5%, 40.5%, 40.8%, and 95.4% for $MgCl_2$, $MgSO_4$, NaCl, and Na_2SO_4 at neutral pH (Zhou et al. 2014). TFC membranes with organically bridged silica deposited on a commercial polymeric membrane (NTR-7450) using low-temperature sol–gel spin-coating and curing were assessed for their vapor permeation dehydration of water-isopropanol solutions (Gong et al. 2014); the results showed a water flux of 2.3 kg/(m^2 h), with markedly enhanced separation factor of 2500. Further, interfacial polymerization of PEI and TMC onto a microporous polyethersulfone support improved membrane performance increasing salt rejection (95.1% for $MgCl_2$, 94.4% for $MgSO_4$, 85.1% for NaCl, and 80.5% for Na_2SO_4) and pure water permeation flux [24.5 L/(m^2h)] (Wu et al. 2014). Poly(vinyl alcohol)/poly(vinylidene fluoride) composite membranes modified with TiO_2 were prepared through dip-coating and applied for dye removal and wastewater treatment (Li et al. 2014); the membranes showed superior performance with enhanced dye removal, salt rejection, and antifouling properties.

Since nanomaterial incorporation can effectively improve the properties of materials due to their size and characteristics (Singh et al. 2013), magnetite nanoparticles (MNPs) have been explored as a potential additive in polymeric composites (Akinay et al. 2018; Zhang et al. 2012; Li et al. 2011). MNPs can enhance the properties of materials, particularly when they are well dispersed within the polymeric composite. MNPs have promising properties as developed surface area, colloidal stability and low toxicity (Kydralieva et al. 2016). The ease of synthesis of MNPs and their unique physicochemical properties (large surface area, synergistic effect on materials mechanical, thermal, magnetic properties and highly active surface groups) lead to advanced applications. (Bustamante-Torres et al 2022). A few studies have reported that the incorporation of MNPs during membrane fabrication greatly enhanced properties desirable for various applications.

In this study, cellulose nitrate (CN) membranes were modified through interfacial surface polymerization of TMC, polyvinylpyrrolidone (PVP), and MNPs. Properties of the obtained TFC membranes (CN-TMC/PVP–MNP) were optimized in terms of reaction time, PVP concentration, and MNPs content to enhance their performance. Structural and surface properties of the produced membranes were analyzed using FTIR, SEM, Inverted phase contrast and AFM. Membrane performance was assessed based on pure water permeation (PWP), salt rejection, antifouling behavior, and surface zeta potential.

Experimental

Materials

Cellulose nitrate (CN) membranes with a diameter of 47 mm and pore size of 0.45 µm were purchased from GVS, USA. m-Phenylenediamine (m-MPD) and trimesoyl chloride (TMC) were obtained from Sigma Aldrich. Hexane and dimethylformamide (DMF) as solvents were obtained from Acros Organics.

Preparation of MNPs

MNPs were prepared as follows. Ferrous sulfate (1 g/100 mL) was slowly (1 mL/10 min) titrated with sodium hydroxide (1 mol/L) until reaching a pH of 12. The obtained black suspension was raised to 200 mL with distilled water and placed in a microwave at half power for 10 min. The obtained black MNPs were repeatedly washed with distilled water until reaching a neutral pH, separated via centrifugation, and dried to a constant weight.

Preparation of TFC membranes

CN membranes were soaked in distilled water for 5 min, followed by immersion in m-PDA solution (2 wt% in deionized) for 2 min. PVP solution (1 wt% in DMF) was mixed with various amounts of MNPs, stirred for 1 h, and sonicated for 30 min at ambient temperature (25 °C). The obtained PVP–MNPs solution was mixed with TMC solution (0.15 wt% in hexane) with continuous stirring to obtain the polymerization mixture. The polymerization mixture was dropped onto one side of the pretreated membranes and left for different reaction times (2, 4 or 6 min).

Membrane characterization

Surface structural properties of the fabricated TFC membranes were analyzed using FTIR spectroscopy (NICOLET 6700 Thermo Scientific) at wave number range of 400–4000 cm^{-1} Surface morphological properties of the thin film were analyzed using SEM (JEOL 6340) and the membrane contrast was imaged using Optika phase contrast. Surface roughness of the prepared membranes was assessed using AFM (NT-MDT, Type Next, Russia) in the non-contact mode and the attached NT-MDT software. The membrane porosity ($\varepsilon\%$), was determined using gravimetric procedure, where the ratio of voids volume to the volume of whole membrane was calculated (Ursino et al. 2019). The membrane dry weight and the membrane weight after immersion in kerosene for 24 h was measured after removing excess kerosene. The membrane porosity was calculated as follows:

$$\varepsilon\% = \left\{ \frac{\left(W_{\mathrm{w}} - W_{\mathrm{d}}\right)/\rho_{\mathrm{k}}}{\left(W_{\mathrm{w}} - W_{\mathrm{d}}\right)/\rho_{\mathrm{k}} + \frac{W_{\mathrm{d}}}{\rho_{\mathrm{p}}}} \right\} \tag{1}$$

Membrane performance

Performance of the fabricated membranes was assessed with a laboratory-designed dead-end filtration device. The effective testing membrane area was 12.56 cm^2. Firstly, the membranes were pre-stabilized for 20 min with the feed sample. Appropriate concentrations of salts (500 mg/L $NaCl_2$ and Na_2SO_4) were applied as feed solutions. These solutions were passed through the membrane at 40 psi. Permeation flux (J, L/m^2 h) and rejection (R, %) were calculated using the following equations:

$$J = \frac{V}{A\Delta t} \tag{2}$$

where V is the permeated volume, A is the effective membrane area, and Δt is the permeation time period.

$$R = \left(1 - \frac{C_{\mathrm{p}}}{C_{\mathrm{f}}}\right) \times 100\% \tag{3}$$

where C_{f} is solute concentration in the feed solution and C_{p} is solute concentration in the permeate solution.

Salt solution concentrations before and after permeation were measured using an electrical conductivity meter.

Antifouling experiment

Antifouling properties of the TFC membranes were studied through permeation experiments using an aqueous solution of sodium alginate (SA; 100 mg/L) as a fouling agent. The fouling results of the membranes were presented in terms of the normalized permeate fluxes J_t/J_o, where J_o and J_t are the initial water flux and water flux after time t of the fouling test, respectively. The values of the normalization flux reflected antifouling behavior of the tested membranes and the fouling agent deposition onto the membrane surface.

Furthermore, membrane antifouling and durability were determined based on fouling reversibility and washing. The removal of fouling agent depends on the weak bonding between the fouling molecules and membrane surface. Thus, to analyze membranes stability and durability, membranes are washed and re-applied in repeated fouling experiments. Accordingly, the SA solution was applied as a feed solution until reaching the steady state, followed by the washing of all permeation equipment and the used membrane with distilled water. The washed membrane was tested for pure water permeation to evaluate the pure water flux and determine the flux recovery ratio (FRR %), as below:

$$\mathrm{FRR}\% = \left(\frac{J_{\mathrm{w2}}}{J_{\mathrm{w1}}}\right) \times 100 \tag{4}$$

where J_{w1} and J_{w2} are pure water fluxes before and after the fouling process, respectively.

Results and discussion

Structural and morphological characteristics of the prepared membranes

FTIR spectroscopy of the composite membrane

FTIR spectra of the unmodified CN membrane and the thin-film modified CN-TMC/PVP–MNPs membrane are shown in Fig. 1. The CN membrane spectrum (Fig. 1a) showed a peak at 3750 cm^{-1}, which was assigned to the stretching vibration of the free O–H of cellulose. The peak corresponding to CH_2 vibrations appeared around 3000 cm^{-1}, while the sharp peak corresponding to the H_2O bending mode appeared at 1635 cm^{-1}. The peaks at 2950 and 2920 cm^{-1} were assigned to symmetric and asymmetric CH_2 vibrations of the polymer chains. The CN-TMC/PVP–MNPs membrane spectrum (Fig. 1b) showed a wide peak at 3450 cm^{-1}, which was assigned to the stretching vibration of the O–H of cellulose, water, and PVP. The peak at 2100 cm^{-1} was assigned to the CN bond in PVP, while the peaks at 1500 and 1400 cm^{-1} were assigned to the CH_2 bending mode and NO_2, COO and C–O vibrations. The sharp peak at 570 cm^{-1} was assigned to N–C=O. The characteristic peak corresponding to Fe^{2+}–O^{2-} of MNPs was slightly shifted and appeared at 530 cm^{-1} due to bonding within the thin film (Cornwell

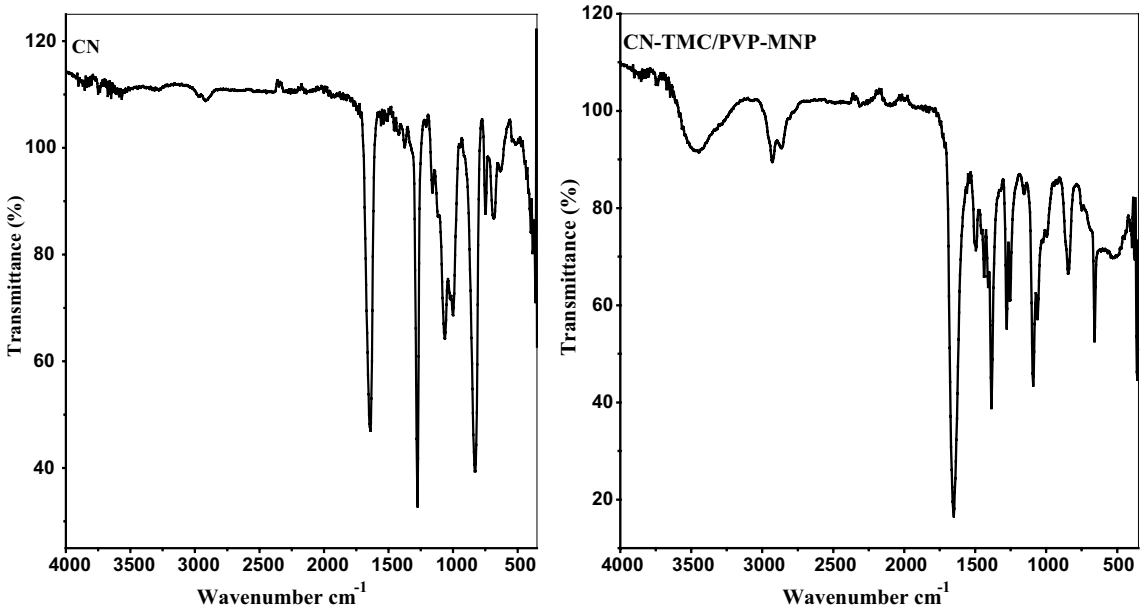

Fig. 1 FTIR spectra of the unmodified CN membrane and the modified CN-TMC/PVP–MNPs membrane with 0.1 wt% MNPs

and Schwertmann 2006; Zheng et al. 2011). The CN-TMC/PVP–MNPs membrane spectrum showed TFC formation on the surface of the supporting CN membrane.

SEM, membrane contrast and AFM of the composite membrane

Scanning electron micrographs of the modified and unmodified CN membranes are shown in Fig. 2a–d. The CN-TMC/PVP–MNPs membranes showed different characteristics from the unmodified CN membranes, as interfacial polymerization formed a coating onto the surface of the modified membranes. As shown in Fig. 2a and c, the CN membrane possesses pores on the surface, while the modified membrane with a thin surface coating (Fig. 2c and d) shows a dense, thick, and a smooth surface. As shown in Fig. 2b and d, the CN-TMC/PVP–MNPs membrane lacks agglomerates, but there is certain folding due to the high surface area of MNPs. MNPs with a large surface area, high surface energy, and high adsorption enter the pores on the surface of the support membrane and enable efficient surface coating with the co-polymer. In micrographs, the CN-TMC/PVP–MNPs membrane shows smaller pores on the surface, and the surface appears more homogeneous with a thin and smooth coating. Moreover, the micrographs of the CN-TMC/PVP–MNPs membrane showed homogeneous distribution of MNPs within the thin surface layer. Thus, MNPs strongly affected the surface properties of the membrane. The membrane contrast images for CN-TMC/PVP (Fig. 2e, f) show uniform film surface, fine structure with no defects on the surface. The images show that the interfacial polymerization has occurred homogenously and equivalently on whole surface of the membrane with no agglomeration, folding or scalloped area.

Atomic force micrographs (AFM) (Fig. 2e and g) of the CN membrane showed symmetric morphology with clear surface roughness. Meanwhile, the micrographs of the CN-TMC/PVP–MNPs membrane (Fig. 2f, and h) showed a dense surface coat with altered roughness due to interfacial polymerization of TFC. The average root-mean-square (RMS) roughness was 258 nm for the modified membrane compared with 153 nm for the unmodified one. These results reflect the formation of a uniform and dense surface film with MNPs distributed within. Thus, interfacial polymerization provides a smooth surface with a dense and thick layer structure.

Contact angle of the composite membranes

The surface contact angles of modified TFC membranes are presented in Fig. 3. The highest pure water contact angle of 85° was obtained for the thin film lacking MNPs, while the angle decreased in the presence of MNPs, reaching 69° at 0.1 wt% MNPs. These results indicate that the inclusion of MNPs improved membrane surface hydrophilicity. This observation can be explained by the fact that the increase in MNPs content enhances PVP concentration, which elevates film thickness and, ultimately, promotes water uptake. Moreover, increasing the content of MNPs with a large surface area and high hydrophilicity nature may markedly enhance surface hydrophilicity. Thin film formation increases surface active groups and polarity, which promotes interactions

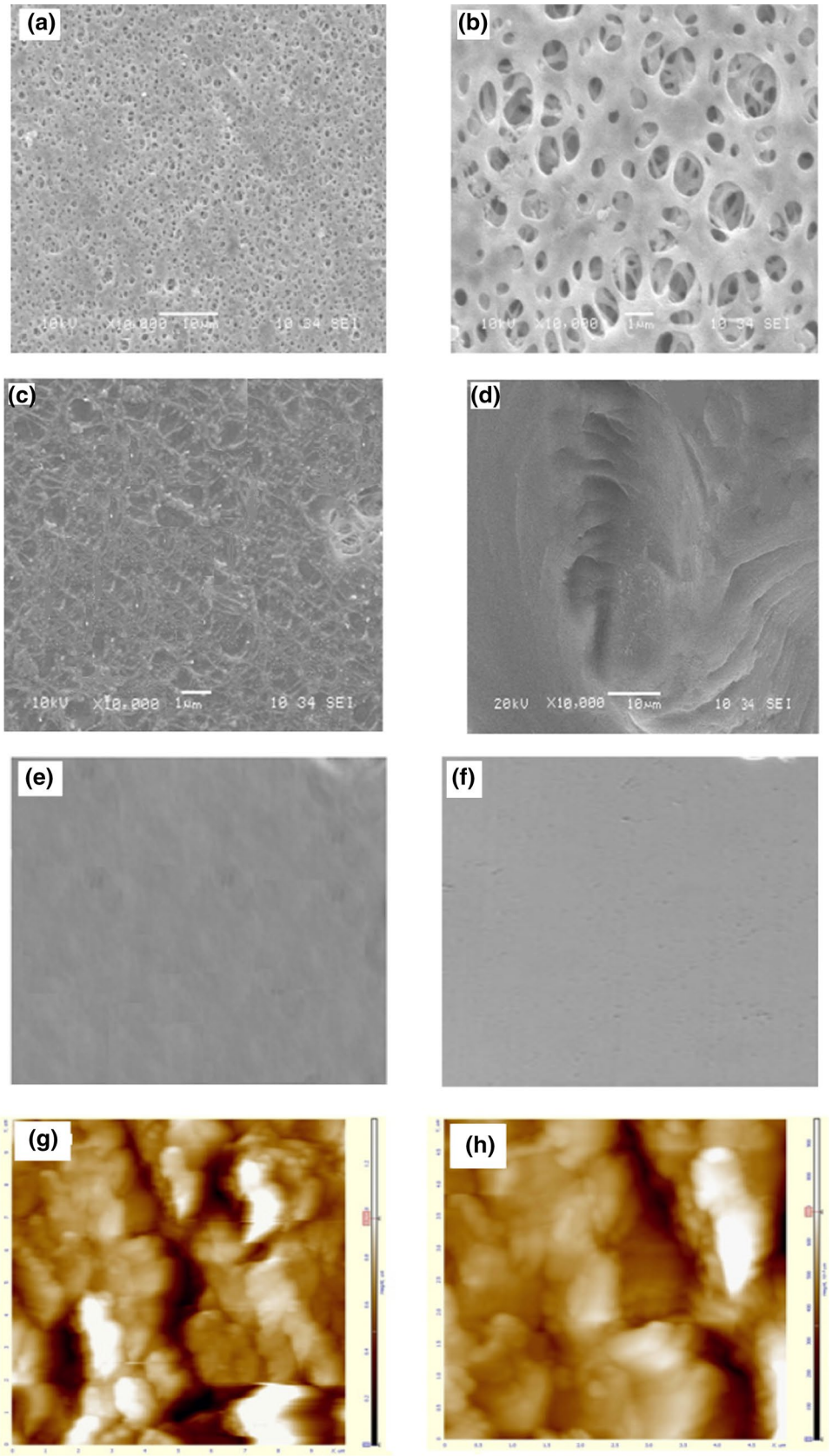

Fig. 2 Scanning electron micrographs of CN (**a**, **c**), and CN-TMC/PVP–MNPs (**b**, **d**) membranes, contrast for CN-TMC/PVP membrane (**e**, **f**) and atomic force micrographs of CN (**e**, **g**) and CN-TMC/PVP–MNPs (**f**, **h**) membranes

Fig. 2 (continued)

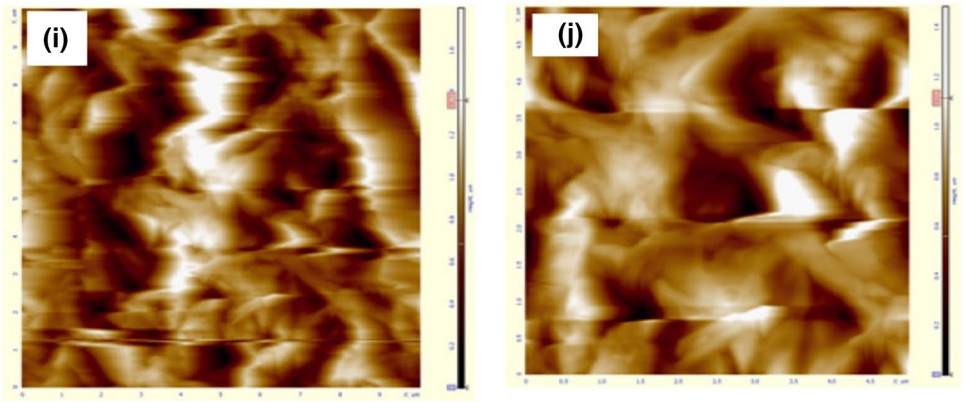

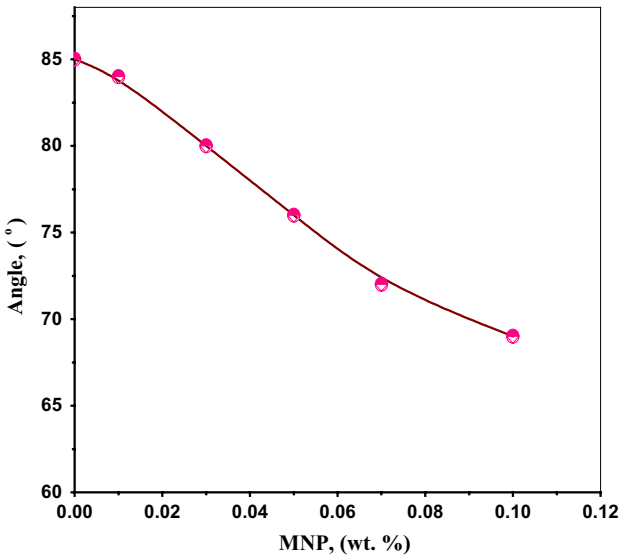

Fig. 3 Effect of MNPs content on the pure water contact angle of CN-TMC/PVP–MNPs membranes

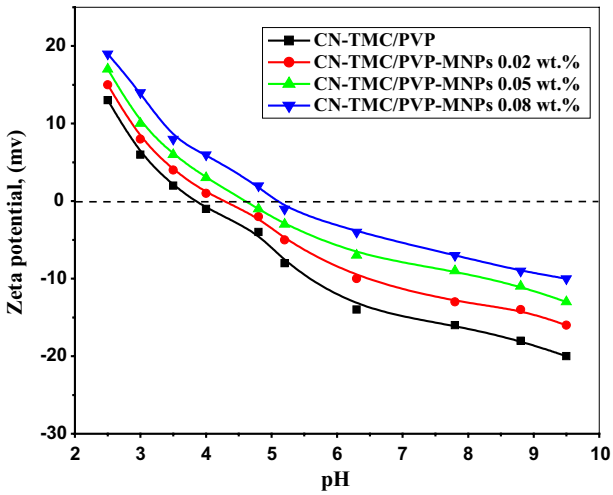

Fig. 4 Zeta potential of the CN-TMC/PVP–MNPs membranes with different MNPs contents

with water molecules through hydrogen bonding and van der Waals forces (Pourjafar et al. 2012; Alghamdi et al. 2019). Furthermore, increased hydrophilicity may effectively improve membrane fouling behavior (Bruggen et al. 2008).

Zeta potential of the composite membrane

The surface charge of membranes strongly affects their characteristics, especially fouling behavior and adsorption properties (Kim et al. 1996; Rodemann and Staude 1995). The adsorption and fouling of materials onto the membrane surface may be affected by its electrostatic interactions with the solutes. Membrane surface charge depends on the dissociation of charged surface groups and pH of the solution (Wilbert et al. 1999). The surface charges of fabricated membranes against solution pH are presented in Fig. 4. Zeta potential decreased with increasing solution pH, which may be explained by the adsorption of OH^- anions and possible dissociation of membrane surface groups. Based on the results in Fig. 4, interfacial polymerization of TMC/PVP thin film affected the surface charge of the CN membrane. Specially, the membrane became negatively charged after a pH of 3.4, and the isoelectric point shifted to approximately 4 due to TMC/PVP polymerization. Moreover, the inclusion of MNPs markedly affected surface charge, as the point of zero charge shifted towards a higher pH value. Nitrogen atoms form quaternary nitrogen species with carboxyl groups of TMC, and the certain electrostatic interactions among surface groups attenuate the negative charge (Liu et al. 2014).

Preparation of CN-TMC/PVP–MNPs composite membranes

Improving the structural and morphological properties of membranes such as higher porosity, pore volume, and film thickness may decrease the hydraulic resistance and consequently affect water permeation. A thin layer plays an important role in the structural and morphological properties

Table 1 Effects of reaction time and PVP concentration on membrane performance

Membrane	Preparation conditions		Membrane performance	
	Reaction time (min)	PVP content (%)	PWP (L/m^2 h bar)	Salt rejection (%) (Na_2SO_4)
CN-NF01	2	0.5	19.6 ± 0.2	80.1 ± 0.7
CN-NF02	4	0.5	17.8 ± 0.3	81.3 ± 0.6
CN-NF03	6	0.5	16.9 ± 0.2	82.1 ± 0.5
CN-NF04	4	0.25	14.8 ± 0.3	83.9 ± 0.6
CN-NF05	4	0.5	12.8 ± 0.4	85.9 ± 0.8
CN-NF06	4	1	11.5 ± 0.3	87.5 ± 0.8

Table 2 Effect of MNPs content on the performance of modified CN membranes

Membrane	Preparation conditions			Membrane performance	
	Reaction time (min)	PVP content (%)	MNPs (%)	PWP (L/m^2 h.bar)	Salt rejection (%) (Na_2SO_4)
CN-NF1	6	0.5	0.02	24.6	84.3
CN-NF2	6	0.5	0.04	21.2	86.8
CN-NF3	6	0.5	0.06	19.3	89.7
CN-NF4	6	0.5	0.08	16.5	94.1
CN-NF5	6	0.5	0.10	13.6	96.8

of the membrane interface and, consequently, determines membrane performance (Ahmad and Ooi 2013). Therefore, membrane performance was assessed as a function of layer thickness. The TFC membrane was prepared through interfacial polymerization of TMC/PVP–MNPs in hexane. The film thickness was controlled by limiting the reaction time between CN and TMC/PVP–MNPs. The reaction time and MNPs content were optimized with respect to membrane performance. The effects of reaction time and PVP concentration on membrane performance were examined and the results are presented in Table 1.

Based on the results in Table 1, both reaction time and PVP concentration, strongly affected CN membrane performance. A longer reaction time affected film thickness, which significantly decreased PWP. The reaction time of 6 min was considered optimum to deliver an appropriate film thickness for providing a PWP of 16.9 L/m^2 h·bar. Moreover, salt rejection of the unmodified CV was clearly improved from 80.1% at a reaction time of 2 min to 82.1% at a reaction time of 6 min, indicating increased thickness of the interfacial polymerized composite film. The role of MNPs in water permeation and salt rejection improvement could be explained due to the diffusion of MNPs through the pores of porous polymeric materials (Bhattacharya 2021). Furthermore, MNPs have surface active groups and have adsorption properties for ions and molecules and which enhances solutes retention. However, higher concentrations of MNPs in the polymeric composite could increase crosslinking between polymeric moieties which provide more surface stiffness, toughness (Romero-Fierro et al. 2022).

Therefore, preparation parameters controlling membrane performance were studied at a fixed reaction time of 6 min and fixed PVP concentration of 0.5%. Moreover, the effect of MNPs content on membrane performance was studied, and the results are presented in Table 2.

Based on results in Table 2, MNPs content of the interfacial thin film significantly affected membrane performance (water flux and salt rejection). The results demonstrate a clear improvement in membrane performance. At the same reaction time and PVP concentration, the presence of MNPs decreased the pure water flux and increased salt rejection of the CN-TMC/PVP–MNPs membrane compared with the CN-TMC/PVP membrane. Effects of MNPs inclusion on PWP are also presented in Fig. 5a. These results could be explained by the properties of MNPs. Specially, MNPs enhance surface hydrophilicity of the interfacial surface layer, consequently promoting water permeation through the thin film (Hu and Mi 2013; Stankovich et al. 2006; Lee et al. 2013). The membrane porosity (ε%), was determined for CN-NF3, CN-NF4 and CN-NF5 and found to be 62, 54 and 44%, respectively. These results reveal that the porosity decreased with increasing MNPs content in the thin-film composite deposited on CN surface, which agreed with the decreased water permeability.

The salt rejection behavior of CN-TMC/PVP–MNPs membranes with different MNPs contents was studied through flow permeation experiments with salt solutions containing NaCl and Na_2SO_4. Based on results in Fig. 5b, the salt rejection of CN-TMC/PVP–MNPs membranes improved with increasing MNPs content. These results could be due to the effect of MNPs on the membrane porosity, as it diffused through the membrane filter micro-pores (Bhattacharya 2021). MNPs additionally have highly active surface groups, which could cause solutes adsorption and increase retention. On the other hand, the presence of MNPs in the composite thin-film increases its viscosity and produces a denser layer which affects the solute rejection. Furthermore, Na_2SO_4 rejection was significantly greater than NaCl rejection. Thus, the rejection of solute ions closely depends on membrane pore size and is strongly affected by both the electrostatic properties of solute ions and membrane surface (Schaep et al. 1998; Peeters et al. 1998). Cations with greater charges show higher membrane affinity and, consequently, greater rejection.

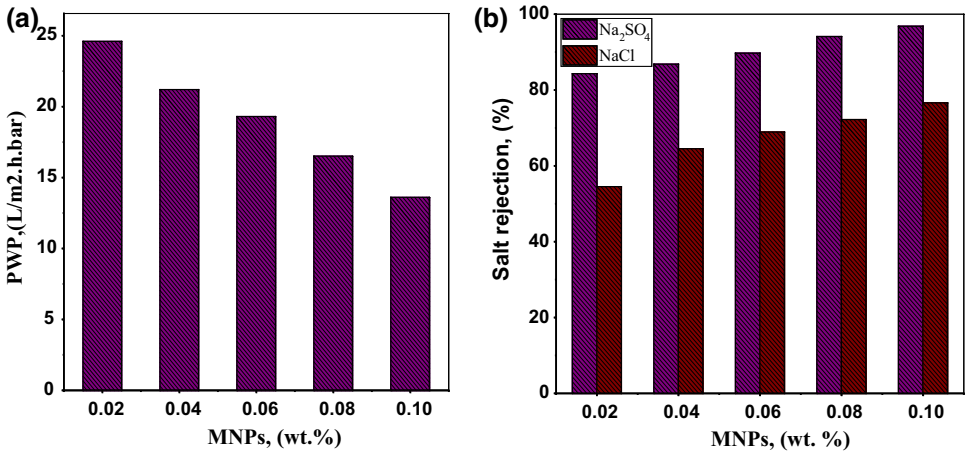

Fig. 5 Effect of MNPs content on the pure water permeability (**a**) and salt rejection (**b**) of the modified CN membrane

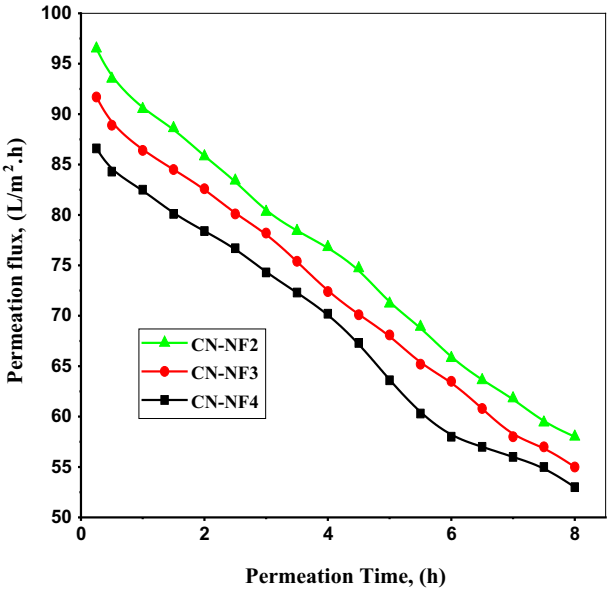

Fig. 6 Effect of permeation time on the permeation flux of Na_2SO_4 solution through CN-TMC/PVP–MNPs membranes with different MNPs contents

Effect of permeation time on permeation flux

The salt rejection behavior for Na_2SO_4 in aqueous solution was further studied using CN-NF2, CN-NF3, and CN-NF4 membranes with different MNPs contents. The permeation of 500 mg/L of Na_2SO_4 was studied at 0.276 MPa and different permeation times, and the results are presented in Fig. 6.

As shown in Fig. 6, the solution fluxes of modified membranes with different MNPs contents gradually decreased with time up to 8 h. The steady-state flux increased with increasing MNPs content, reflecting improvement of the antifouling behavior due to the inclusion of MNPs. These results reflect the antifouling behavior of the modified TFC membrane toward salt solutions and highlight its potential application for heavy metal removal and pollutant rejection. Additionally, as shown in Table 3, salt rejection of the prepared TFC membranes was improved. These observations may be explained by the improvement of surface properties due to thin-film polymerization and MNPs addition. Moreover, under the present experimental conditions, electrostatic interaction likely produced a marked effect.

Table 3 Steady-state salt rejection and permeation fluxes of CN-TMC/PVP–MNPs membranes

Membrane	Steady-state flux (L/m^2 h)	Steady-state removal of Na_2SO_4 (%)
CN-NF2	53	86.7
CN-NF3	55	90.1
CN-NF4	58	94.3

Antifouling behavior of CN-TMC/PVP–MNPs membrane

The antifouling behaviors of fabricated CN-NF3 and CN-NF4 membranes were evaluated during the permeation of 100 mg/L aqueous SA solution at pH 7.0 and of 25 °C. The molecular size of the applied fouling agent is larger than the NF membrane pore size; therefore, it cannot pass through the membrane pores during solution permeation, leading to the fouling of the membrane surface. Surface fouling was performed at a permeation flux of 80 L/m^2·h to verify the required permeation-driving hydrodynamic force. Normalized fluxes (J_t/J_o) of the studied membranes are presented in Fig. 7.

As shown in Fig. 7, membrane flux for the SA solution sharply decreased at first, followed by a slow decrease over time. These observations may be attributed to the deposition of fouling agent on the membrane surface until reaching the steady state. The steady-state flux of aqueous SA solution decreased at a rate of about 6% for the CN-NF4 membrane

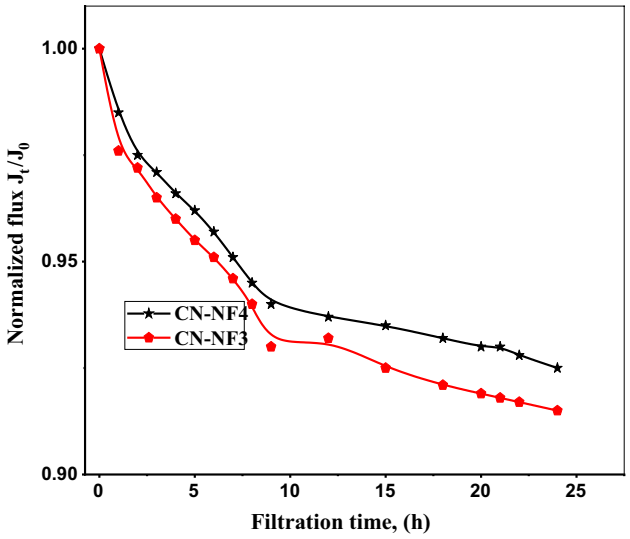

Fig. 7 Effect of filtration time on the normalized flux of SA solution through CN-TMC/PVP–MNPs membranes

Table 4 Flux recovery ratios of the CN-NF3 and CN-NF4 membranes after repeated SA fouling-washing cycles

Fouling-cleaning cycles	FRR%	
	CN-NF3 (%)	CN-NF4 (%)
1st cycle	97	98
2nd cycle	93	94
3rd cycle	89	91
4th cycle	81	83

and 8% for the CN-NF3 membrane. These findings indicate the effect of MNPs content in the interfacially polymerized thin film on the surface properties of membrane for improving its fouling behavior. The membrane with a higher MNPs content showed a better performance in fouling resistance. Fouling agents are adsorbed onto the membrane surface via hydrophobic interactions, hydrogen bonds, electrostatic interactions, and van der Waals forces. Consequently, antifouling properties can be improved by decreasing the adsorption driving forces and enhancing the repulsion effect of the membrane surface on the fouling molecules (Bruggen et al. 2008; Al-Amoudi and Lovitt 2007). Notably, at the specified testing conditions, the membrane surfaces are more negatively charged; thus, stronger electrostatic repulsive forces may act between the membrane surface and fouling agent, resulting in a weaker fouling effect.

Furthermore, to analyze flux recovery ratio (FRR %), membranes stability, and durability, membranes are washed and re-applied in repeated fouling experiments. As shown in Table 4, the inclusion of MNPs in the thin film improved antifouling properties, providing higher FRRs. This improvement of antifouling properties may be related to the increased hydrophilic properties of the composite surface layer, which may inhibit the interaction between the fouling molecules and hydrophobic membrane surface. Surface hydrophilicity determines surface adsorption behavior (Khorshidi et al. 2016; El-Zahhar 2019). The increase in hydrophilicity by the presence of MNPs was confirmed based on the decrease in water contact angle with increasing MNPs content. Based on results in Table 4, the CN-NF3 and CN-NF4 membranes were stable until the fourth fouling-washing cycle. Overall, the CN-TMC/PVP–MNPs membranes showed increased stability, durability, and FRRs, indicating their possible application for water desalination and treatment.

Conclusion

Nanofiltration TFC membranes were fabricated via modified interfacial polymerization of TMC/PVP–MNPs on the surface of a porous CN support. The optimum preparation conditions are a reaction time of 6 min, PVP concentration of 0.5 wt%, and MNPs content of 0.1 wt%. Structural and morphological analyses revealed differences between the unmodified CN and the modified CN-TMC/PVP–MNPs membranes. The pure water contact angle of the modified membrane (with 0.1 wt% MNPs) was decreased to 69° compared with 85° of the unmodified membrane. The zeta potential of the CN-TMC/PVP–MNPs membrane significantly varied with increase in MNPs content. Although the PWP decreased with increasing MNPs content, membrane performance was superior due to enhanced salts rejection and clearly improved stability, durability, and antifouling performance.

Acknowledgements The authors extend their appreciation to the Deanship of Scientific Research at King Khalid University for funding this work through research groups program under grant number R.G.P. 1/11/42.

Declarations

Conflict of interest On behalf of all authors, the corresponding author states that there is no conflict of interest.

References

Ahmad AL, Ooi BS (2013) Properties–performance of thin-film composites membrane: study on trimesoylchloride content and polymerization time. J Membr Sci 255:67–77. https://doi.org/10.1016/j.memsci.2005.01.021

Akinay Y, Hayat F, Çakir M, Akin E (2018) Magnetic and microwave absorption properties of PVB/Fe_3O_4 and PVB/$NiFe_2O_4$

composites. Polym Compos 39:3418–3423. https://doi.org/10.1002/pc.24359
Al-Amoudi A, Lovitt RW (2007) Fouling strategies and the cleaning system of NF membranes and factors affecting cleaning efficiency. J Membr Sci 303:4–28. https://doi.org/10.1016/j.memsci.2007.06.002
Alghamdi MM, El-Zahhar AA, Asiri BM (2019) Incorporation of magnetite nanoparticles in poly(vinyl chloride) microfiltration membrane for improving antifouling property and desalination performance. Desalination Water Treat 165:54–62. https://doi.org/10.5004/dwt.2019.24495
Bai L, Liu Y, Ding A, Ren N, Li G, Liang H (2019) Fabrication and characterization of thin-film composite (TFC) nanofiltration membranes incorporated with cellulose nanocrystals (CNCs) for enhanced desalination performance and dye removal. Chem Eng J 358:1519–1528. https://doi.org/10.1016/j.cej.2018.10.147
Bhattacharya S (2021) Nanostructures in gene delivery. In: Bajpai A, Saini R (eds) Advances in polymeric nanomaterials for biomedical applications, 1st edn. Elsevier Inc., Cham, pp. 101–135. ISBN 978–0–12–814657–6
Bruggen BV, Mänttäri M, Nyström M (2008) Drawbacks of applying nanofiltration and how to avoid them: a review. Sep Purif Technol 63:251–263. https://doi.org/10.1016/j.seppur.2008.05.010
Bustamante-Torres M, Romero-Fierro D, Estrella-Nuñez J, Arcentales-Vera B, Chichande-Proaño E, Bucio E (2022) Polymeric composite of magnetite iron oxide nanoparticles and their application in biomedicine: a review. Polymers 14:752. https://doi.org/10.3390/polym14040752
Cheng L, Liu G, Zhao J, Jin W (2021) Two-dimensional-material membranes: manipulating the transport pathway for molecular separation. Acc Mater Res. https://doi.org/10.1021/accountsmr.0c00092
Chung TS, Zhang S, Wang KY, Su J, Ling MM (2012) Forward osmosis processes: yesterday, today and tomorrow. Desalination 287:78–81. https://doi.org/10.1016/j/desal.2010.12.019
Cornwell RM, Schwertmann U (2006) The iron oxides structure, properties, reactions, occurrences and uses, 2nd edn. Wiley VCH Verlag GmbH & Co. KGaA, Weinheim
Deng L, Li S, Qin Y, Zhang L, Chen H, Chang Z, Hu Y (2021) Fabrication of antifouling thin-film composite nanofiltration membrane via surface grafting of polyethyleneimine followed by zwitterionic modification. J Membr Sci 619:118564. https://doi.org/10.1016/j.memsci.2020.118564
Dong L, Huang X, Wang Z, Yang Z, Wang X, Tang CY (2016) A thin-film nanocomposite nanofiltration membrane prepared on a support with in situ embedded zeolite nanoparticles. Sep Purif Technol 166:230–239. https://doi.org/10.1016/j.seppur.2016.04.043
El-Zahhar AA, Alghamdi MM, Asiri BM (2019) Poly (vinyl chloride)-MMT composite membranes with enhanced properties and separation performance. Desalination Water Treat 155:381–389. https://doi.org/10.5004/dwt.2019.24075
Geoffrey HSL, Geise M, Miller DJ, Freeman BD, Mcgrath JE, Paul DR (2010) Water purification by membranes: the role of polymer science. J Polym Sci Part B Polym Phys 48:1685–1718. https://doi.org/10.1002/polb.22037
Gong G, Wang J, Nagasawa H, Kanezashi M, Yoshioka T, Tsuru T (2014) Synthesis and characterization of alayered-hybrid membrane consisting of an organosilica separation layer on a polymeric nanofiltration membrane. J Membr Sci 472:19–28. https://doi.org/10.1016/j.memsci.2014.08.030
Han J, Yang D, Zhang S, Wang L, Jian X (2014) Preparation and performance of SPPES/PPES hollow fiber composite nanofiltration membrane with high temperature resistance. Desalination 350:95–101. https://doi.org/10.1016/j.desal.2014.06.029
Hu M, Mi B (2013) Enabling graphene oxide nanosheets as water separation membranes. Environ Sci Technol 47:3715–3723. https://doi.org/10.1021/es400571g
Joseph N, Ahmadiannamini P, Jishna PS, Volodin A, Vankelecom IFJ (2015) "Up-scaling" potential for polyelectrolyte multilayer membranes. J Membr Sci 492:271–280
Khorshidi B, Hajinasiri J, Ma G, Bhattacharjee S, Sadrzadeh M (2016) Thermally resistant and electrically conductive PES/ITO nanocomposite membrane. J Membr Sci 500:151–160. https://doi.org/10.1016/j.memsci.2015.11.015
Kim KJ, Fane AG, Nystrom M, Pihlajamaki A, Bowen WR, Mukhtar H (1996) Evaluation of electro osmosis and streaming potential for measurement of electric charges of polymeric membranes. J Membr Sci 116:149–159. https://doi.org/10.1016/0376-7388(96)00038-5
Kim S, Chu KH, Al-Hamadani YAJ, Park CM, Jang M, Kim DH, Yu M, Heo J, Yoon Y (2018) Removal of contaminants of emerging concern by membranes in water and wastewater: a review. Chem Eng J 335:896–914. https://doi.org/10.1016/j.cej.2017.11.044
Kumar S, Garg A, Chowdhuri A (2019) Sonication effect on graphene oxide (GO) membranes for water purification applications. Mater Res Express 6:085620. https://doi.org/10.1088/2053-1591/ab1ffd
Kydralieva KA, Dzhardimalieva GI, Yurishcheva AA, Jorobekova SJ (2016) Nanoparticles of magnetite in polymer matrices: synthesis and properties. J Inorg Organomet Polym 26(5):921–1106. https://doi.org/10.1007/s10904-016-0436-1
Lau WJ, Ismail AF, Misdan N, Kassim MA (2012) A recent progress in thin film composite membrane: a review. Desalination 287:190–199. https://doi.org/10.1016/j.desal.2011.04.004
Lee J, Chae HR, Won YJ, Lee K, Lee CH, Lee HH, Kim IC, Lee JM (2013) Graphene oxide nanoplatelets composite membrane with hydrophilic and antifouling properties for wastewater treatment. J Membr Sci 448:223–230. https://doi.org/10.1016/j.memsci.2013.08.017
Li XA, Zhang B, Ju CH, Han XJ, Du YC, Xu P (2011) Morphology-controlled synthesis and electromagnetic properties of porous Fe_3O_4 nanostructures from iron alkoxide precursors. J Phys Chem C 115:12350–12357. https://doi.org/10.1021/jp203147q
Li X, Chen Y, Hu X, Zhang Y, Hu L (2014) Desalination of dye solution utilizing PVA/PVDF hollow fiber composite membrane modified withTiO2 nanoparticles. J Membr Sci 471:118–129. https://doi.org/10.1016/j.memsci.2014.08.018
Liu G, Gui S, Zhou H, Zeng F, Zhou Y, Ye H (2014) A strong adsorbent for Cu^{2+}: graphene oxide odified with triethanolamine. Dalt Trans 43:6977–6980. https://doi.org/10.1039/C4DT00063C
Ma X, Yang Z, Yao Z, Guo H, Xu Z, Tang CY (2019) Tuning roughness features of thin film composite polyamide membranes for simultaneously enhanced permeability, selectivity and antifouling performance. J Colloid Interface Sci 540:382–388. https://doi.org/10.1016/j.jcis.2019.01.033
Ormanci AT, Tas CE, Keskin B, Billur E, Ozbulut S, Turker T, Imer D, Tufekci N, Menceloglu YZ, Unal S, Koyuncu I (2020) Thin-film composite nanofiltration membranes with high flux and dye rejection fabricated from disulfonated diamine monomer. J Membr Sci 60:118172. https://doi.org/10.1016/j.memsci.2020.118172
Peeters JM, Boom JP, Mulder MH, Strathmann H (1998) Retention measurements of nanofiltration membranes with electrolyte solutions. J Membr Sci 145:199–209. https://doi.org/10.1016/S0376-7388(98)00079-9
Pourjafar S, Rahimpour A, Jahanshahi M (2012) Synthesis and characterization of PVA/PES thin film composite nanofiltration membrane modified with TiO_2 nanoparticles for better performance and surface properties. J Ind Eng Chem 18:1398–1405. https://doi.org/10.1016/j.jiec.2012.01.041
Rathore AS, Shirke A (2011) Recent developments in membrane-based separations in biotechnology processes: review. Prep Biochem 41:398–421. https://doi.org/10.1080/10826068.2011.613976

Rodemann K, Staude E (1995) Electrokinetic characterization of porous membranes made from epoxidized polysulfone. J Membr Sci 104:147–155. https://doi.org/10.1016/0376-7388(95)00024-7

Romero-Fierro D, Camacho-Cruz L, Bustamante-Torres M, Hidalgo-Bonilla S, Bucio E (2022) Modification of cotton gauzes with poly(acrylic acid) and poly(methacrylic acid) using gamma radiation for drug loading studies. Radiat Phys Chem 190:109787. https://doi.org/10.1016/j.radphyschem.2021.109787

Schaep J, Van DB, Vandecasteele C, Wilms D (1998) Influence of ion size and charge in nanofiltration. Sep Purif Technol 14:155–162. https://doi.org/10.1016/S1383-5866(98)00070-7

Singh A, Shirolkar M, Limaye MV, Gokhale S, Malek CK, Kulkarni SK (2013) A magnetic nano-composite soft polymeric membrane. Microsyst Technol 19:409–418. https://doi.org/10.1007/s00542-012-1646-2

Stankovich S, Dikin DA, Dommett GH, Kohlhaas KM, Zimney EJ, Stach EA, Piner RD, Nguyen ST, Ruoff RS (2006) Graphene-based composite materials. Nature 442:282–286. https://doi.org/10.1038/nature04969

Ursino C, Di Nicolo E, Gabriele B, Criscuoli A, Figoli A (2019) Development of a novel perfluoropolyether (PFPE) hydrophobic/hydrophilic coated membranes for water treatment. J Membr Sci 581:58–71. https://doi.org/10.1016/j.memsci.2019.03.041

Wei X, Kong X, Yang J, Zhang G, Chen J, Wang J (2013) Structure influence of hyperbranched polyester on structure and properties of synthesized nanofiltration membranes. J Membr Sci 440:67–76. https://doi.org/10.1016/j.memsci.2013.03.034

Wilbert MC, Delagah S, Pellegrino J (1999) Variance of streaming potential measurements. J Membr Sci 161:247–261. https://doi.org/10.1016/S0376-7388(99)00117-9

Wu D, Huang Y, Yu S, Lawless D, Feng X (2014) Thin film composite nanofiltration membranes assembled layer-by-layer via interfacial polymerization from polyethylenimine and trimesoylchloride. J Membr Sci 472:141–153. https://doi.org/10.1016/j.memsci.2014.08.055

Xu Y, Lin J, Gao C, Bart V, Shen Q, Shao H, Shen J (2017) Preparation of high-flux nanoporous solvent resistant PAN membrane with potential fractionation of dyes and Na_2SO_4. Ind Eng Chem Res 56:11967–11976. https://doi.org/10.1021/acs.iecr.7b03409

Ye CC, Zhao FY, Wu JK, Weng XD, Zheng PY, Mi YF, An QF, Gao CJ (2017) Sulfated polyelectrolyte complex nanoparticles structured nanoflitration membrane for dye desalination. Chem Eng J 307:526–536. https://doi.org/10.1016/j.cej.2016.08.122

Zhang SJ, Liu XH, Zhou LP, Peng WJ (2012) Magnetite nanostructures: One-pot synthesis, superparamagnetic property and application in magnetic resonance imaging. Mater Lett 68:243–246. https://doi.org/10.1016/j.matlet.2011.10.070

Zhao S, Ba C, Yao Y, Zheng W, Economy J, Wang P (2018) Removal of antibiotics using polyethylenimine cross-linked nanofiltration membranes: relating membrane performance to surface charge characteristics. Chem Eng J 335:101–109. https://doi.org/10.1016/j.cej.2017.10.140

Zheng L, Su W, Qi Z, Xu Y, Zhou M, Xie Y (2011) First-order metal-insulator transition and infrared identification of shape-controlled magnetite nanocrystals. Nanotechnology 22:485706. https://doi.org/10.1088/0957-4484/22/48/485706

Zhou C, Shi Y, Sun C, Yu S, Liu M, Gao C (2014) Thin-film composite membranes formed by interfacial polymerization with natural material sericin and trimesoylchloride for nanofiltration. J Membr Sci 471:381–391. https://doi.org/10.1016/j.memsci.2014.08.033